OXFORD

Human Molecular Genetics, 2024, 1–13
https://doi.org/10.1093/hmg/ddae028
Original Article

Comparative analysis of *in-silico* tools in identifying pathogenic variants in dominant inherited retinal diseases

Daniel C. Brock[1,2], Meng Wang[1], Hafiz Muhammad Jafar Hussain[1], David E. Rauch[1], Molly Marra[3], Mark E. Pennesi[3], Paul Yang[3], Lesley Everett[3], Radwan S. Ajlan[4], Jason Colbert[4], Fernanda Belga Ottoni Porto[5,6,7], Anna Matynia[8], Michael B. Gorin[9,10], Robert K Koenekoop[11], Irma Lopez[11], Ruifang Sui[12], Gang Zou[13], Yumei Li[1,14], Rui Chen[1,14,*]

[1]Department of Molecular and Human Genetics, Baylor College of Medicine, One Baylor Plaza, Houston, TX 77030, United States
[2]Medical Scientist Training Program, Baylor College of Medicine, One Baylor Plaza, Houston, TX 77030, United States
[3]Department of Ophthalmology, Casey Eye Institute, Oregon Health & Science University, 515 SW Campus Drive, Portland, OR 97239, United States
[4]Department of Ophthalmology, University of Kansas School of Medicine, 3901 Rainbow Blvd, Kansas City, KS 66160, United States
[5]INRET Clínica e Centro de Pesquisa, Rua dos Otoni, 735/507 - Santa Efigênia, Belo Horizonte, MG 30150270, Brazil
[6]Department of Ophthalmology, Santa Casa de Misericórdia de Belo Horizonte, Av. Francisco Sales, 1111 - Santa Efigênia, Belo Horizonte, MG 30150221, Brazil
[7]Centro Oftalmológico de Minas Gerais, R. Santa Catarina, 941 - Lourdes, Belo Horizonte, MG 30180070, Brazil
[8]College of Optometry, University of Houston, 4401 Martin Luther King Boulevard, Houston, TX 77004, United States
[9]Jules Stein Eye Institute, University of California Los Angeles, 100 Stein Plaza, Los Angeles, CA 90095, United States
[10]Department of Ophthalmology, University of California Los Angeles David Geffen School of Medicine, 10833 Le Conte Ave, Los Angeles, CA 90095, United States
[11]McGill Ocular Genetics Laboratory and Centre, Department of Paediatric Surgery, Human Genetics, and Ophthalmology, McGill University Health Centre, 5252 Boul de Maisonneuve ouest, Montreal, QC H4A 3S5, Canada
[12]Department of Ophthalmology, Peking Union Medical College Hospital, Peking Union Medical College, Chinese Academy of Medical Sciences, WC67+HW Dongcheng, Beijing 100005, China
[13]Department of Ophthalmology, Ningxia Eye Hospital, People's Hospital of Ningxia Hui Autonomous Region, First Affiliated Hospital of Northwest University for Nationalities, Ningxia Clinical Research Center on Diseases of Blindness in Eye, F4RJ+43 Xixia District, Yinchuan, Ningxia, China
[14]Human Genome Sequencing Center, Baylor College of Medicine, One Baylor Plaza, Houston, TX 77030, United States
*Corresponding author. Professor Rui Chen, Department of Molecular and Human Genetics, Baylor College of Medicine, Houston, TX, 77030, United States. E-mail: ruichen@bcm.edu

Abstract

Inherited retinal diseases (IRDs) are a group of rare genetic eye conditions that cause blindness. Despite progress in identifying genes associated with IRDs, improvements are necessary for classifying rare autosomal dominant (AD) disorders. AD diseases are highly heterogenous, with causal variants being restricted to specific amino acid changes within certain protein domains, making AD conditions difficult to classify. Here, we aim to determine the top-performing *in-silico* tools for predicting the pathogenicity of AD IRD variants. We annotated variants from ClinVar and benchmarked 39 variant classifier tools on IRD genes, split by inheritance pattern. Using area-under-the-curve (AUC) analysis, we determined the top-performing tools and defined thresholds for variant pathogenicity. Top-performing tools were assessed using genome sequencing on a cohort of participants with IRDs of unknown etiology. MutScore achieved the highest accuracy within AD genes, yielding an AUC of 0.969. When filtering for AD gain-of-function and dominant negative variants, BayesDel had the highest accuracy with an AUC of 0.997. Five participants with variants in *NR2E3*, *RHO*, *GUCA1A*, and *GUCY2D* were confirmed to have dominantly inherited disease based on pedigree, phenotype, and segregation analysis. We identified two uncharacterized variants in *GUCA1A* (c.428T>A, p.Ile143Thr) and *RHO* (c.631C>G, p.His211Asp) in three participants. Our findings support using a multi-classifier approach comprised of new missense classifier tools to identify pathogenic variants in participants with AD IRDs. Our results provide a foundation for improved genetic diagnosis for people with IRDs.

Keywords: inherited retinal diseases; autosomal dominant; variant classification; genetic diagnosis; next-generation sequencing

Introduction

Inherited retinal diseases (IRDs) comprise a heterogenous group of rare genetic conditions characterized by pathogenic variants in proteins governing retinal function, leading to irreversible blindness for millions of patients worldwide. There exists high phenotypic and genotypic heterogeneity in patients with IRDs, with over 320 genes associated with autosomal dominant, autosomal recessive, X-linked, and mitochondrial inheritance patterns [1]. Autosomal dominant (AD) IRDs frequently impact several generations in a family, with a child having a 50% chance of inheriting a disease-causing allele from their affected parent. Given the significant generational history of blindness in families impacted by AD IRDs, affected individuals are likely to seek family planning and genetic counseling to identify the underlying etiology of their condition.

Next generation sequencing (NGS) technologies are poised to revolutionize precision medicine due to being both cost- and time-effective and have become a gold standard in diagnosing patients with IRDs [2–4]. Despite the increasing clinical accessibility of NGS, there continues to exist a disparity between sequencing

Received: January 8, 2024. **Revised:** February 16, 2024. **Accepted:** February 19, 2024

patients and accurately classifying disease-causing variants [5]. This is especially true for rare AD diseases, where the etiology of variants is highly heterogenous and frequently restricted to certain amino acid changes within specific protein domains, resulting in either a loss- or gain-of-function [6]. In contrast, autosomal recessive (AR) diseases are almost universally a result of biallelic loss-of-function variants. As gene therapies and clinical trials for IRDs continue to expand, it is crucial that patients and family members impacted by AD IRDs receive an accurate genetic diagnosis [7].

Currently, *in-silico* tools, such as PolyPhen-2 [8], SIFT [9], and CADD [10], are commonly used in clinical practice to predict variant pathogenicity for IRD patients. These tools are designed to predict variants that negatively impact protein function based on features such as amino acid substitutions, surrounding sequence context, and conservation. Newer tools utilize innovative machine learning techniques, incorporating additional features, such as allele frequency, gene-specific variant clustering, and scores generated from other classifiers to form metapredictors [11–15]. These tools also train on larger datasets, resulting in an overall performance gain compared to historically utilized classifiers [16]. Nevertheless, due to the diverse molecular characteristics of AD variants, it remains uncertain whether *in-silico* predictors can maintain consistent performance between recessive and dominant variants. In this study, we performed benchmarking of newer and commonly utilized classifiers with annotated variants gathered from ClinVar. The top-performing tools were applied to genome sequencing data on a cohort of over 1000 research participants with IRDs of unknown etiology to identify candidate pathogenic AD IRD variants with subsequent validation using clinical phenotyping and segregation testing.

Results

Benchmarking classifiers on IRD genes

We identified 3322 IRD variants from ClinVar which matched our filtering criteria and were classified as pathogenic or likely pathogenic (PLP) and benign or likely benign (BLB) (Fig. 1). Using the annotations as ground truth, variants were grouped by inheritance pattern gathered from the Retinal Information Network, RetNet [1], and 39 different variant classifier tools were benchmarked (Supplemental Table 1). Out of these 39 classifiers, MutScore, MetaRNN, ClinPred, BaysDel_addAF, REVEL, and VEST4 consistently ranked as the top performing models (Table 1). For comparison purposes, classifiers used traditionally in clinical practice, such as SIFT, Polyphen2, and CADD, were included for reference. Benchmarking classifiers using a total of 1524 AD ClinVar variants revealed that MutScore had the highest performance, with an AUC of 0.969 (Fig. 2A). Similar high performance is observed when 2392 AR ClinVar variants were benchmarked, with ClinPred having the highest performance with an AUC of 0.984 (Fig. 2B). For further categorization, AD variants were split into AD haploinsufficiency and AD gain-of-function (GOF) & dominant negative (DN) categories without overlap from variants with AR genes. AD genes were considered haploinsufficient if their allele frequency was $< 1e^{-3}$ and probability of loss-of-function intolerance score (pLI) > 0.90, while AD genes were considered GOF or DN if their allele frequency was $< 1e^{-5}$ and pLI < 0.90. Interestingly, high performance was achieved despite the dramatic difference in the molecular nature of these types of variants. BayesDel_addAF was the top performing classifier when benchmarking 728 variants within AD haploinsufficiency genes, with an AUC of 0.972 (Fig. 2C). BayesDel_addAF was also the top performing classifier when benchmarking 156 variants within AD GOF & DN genes, with an AUC of 0.997 (Fig. 2D). Notably, there was greater variation in performance among classifiers when benchmarking variants within AD GOF & DN genes with a mean AUC difference of 0.139 between top-performing classifiers and tools used traditionally in clinical practice, such as SIFT, CADD, and Polyphen2 ($P = 0.016$) (Supplemental Fig. 1). In comparison, the mean difference in AUC between top-performing and traditional tools was 0.095 when comparing all AD variants ($P = 1.88e^{-5}$) and 0.065 when comparing only variants within AD haploinsufficiency genes ($P = 0.0096$). Therefore, larger improvements in classifier accuracy were observed in newer tools for predicting GOF & DN variants compared to loss-of-function (LOF) variants.

Defining thresholds for pathogenicity scores

To define likely-pathogenic (LP) and likely-benign (LB) variants, we determined upper and lower threshold scores for the six top-performing classifiers (MutScore, MetaRNN, ClinPred, BayesDel_addAF, REVEL, and VEST4). Using all AD variants from ClinVar, we defined the upper threshold used for labeling LP variants as the maximum classifier score representing the point at which 95% of the testing data from ClinVar was accurately confirmed as PLP (Fig. 3). The lower threshold, used for labeling LB variants, was defined as the minimum classifier score representing the point at which 95% of the testing data from ClinVar was accurately confirmed as BLB. Variants with scores falling between the upper and lower thresholds were labeled as variants of unknown significance (VUS). Using these thresholds to determine variant pathogenicity classifications, we annotated rare variants identified from 1013 participants with unsolved IRDs who were sequenced via whole genome sequencing (WGS). 7045 rare variants were detected in IRD genes, of which 5561 were unique. Of these rare variants, 2342 occurred in AD IRD genes, of which 1832 were unique. Most variants were classified as LB as expected, while about 3%–7% of IRD participant variants were classified as LP per top-performing tool. To gauge classifier concordance among top-performing tools, a heatmap was generated with three clusters: LP, LB, and VUS (Supplemental Fig. 2). The high degree of concordance revealed that the majority of tools had agreeing classifications, which resulted in 113 unique AD IRD variants that were selected for further interpretation.

Identification of participants with likely AD IRDs

Of the 1013 unsolved IRD participants and 113 LP variants in AD genes, 22 candidate participants harboring LP variants in AD genes were identified (Supplemental Table 2). For candidate selection, at least three classifier tools had to classify a variant as LP and the variant had to be defined as rare, with an allele frequency less than $1e^{-5}$ for DN and GOF variants and less than $1e^{-3}$ for haploinsufficiency variants. Of these 22 candidates, 5 participants were confirmed to have AD pedigrees, 7 participants had sporadic disease, and 10 participants had no pedigree available at the time of conducting this study (Table 2, Supplemental Table 2). Notably, proband MEP_275, a 75-year-old male diagnosed with retinitis pigmentosa (RP, OMIM: 611131), presented with a paternal family history of RP suggestive of an AD inheritance pattern (Fig. 4A). MEP_275 harbors a heterozygous variant in exon 2 of the *NR2E3* gene (HGNC:7974, NM_014249: c.166G>A), as shown in the IGV plot (Supplemental Fig. 3A). This missense variant in *NR2E3* replaces a conserved glycine residue with arginine at codon 56 (NP_055064: p.Gly56Arg) and is absent in the gnomAD database. Five out of six classifiers, MutScore,

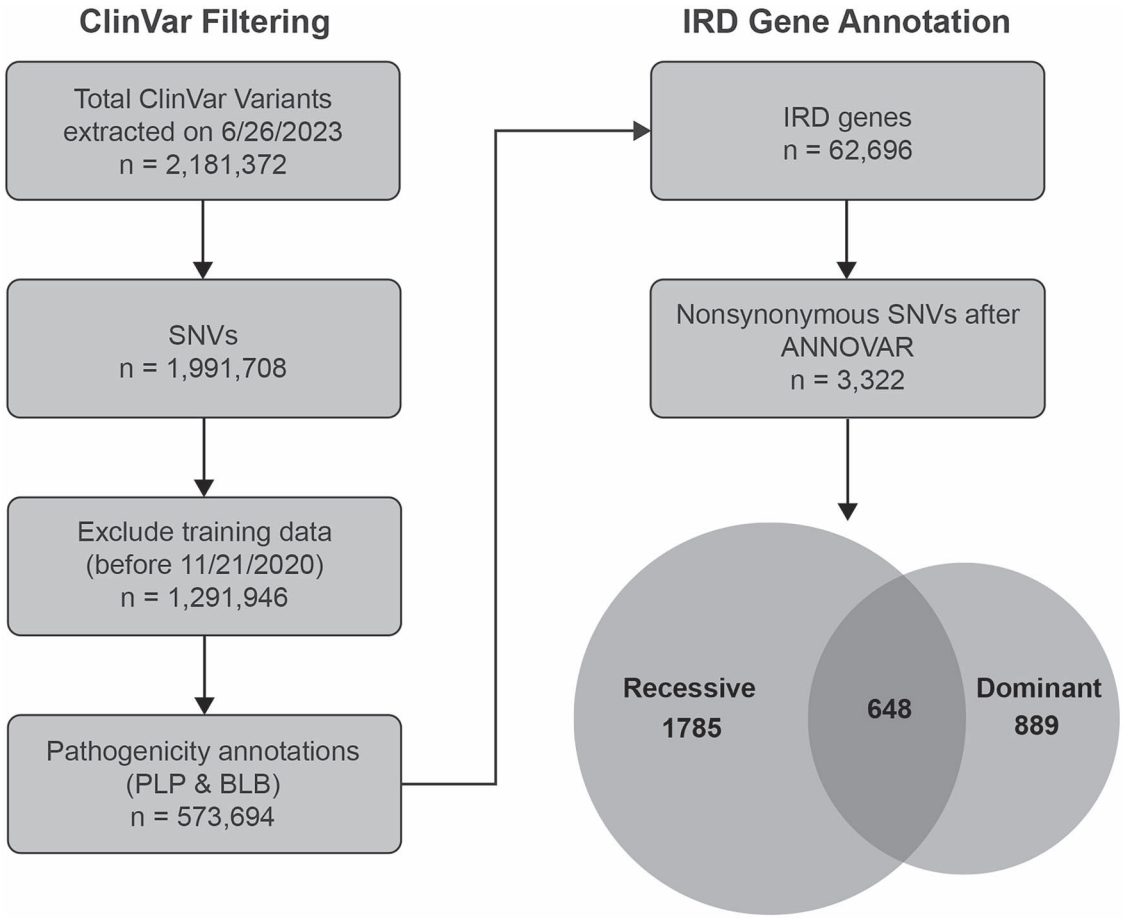

Figure 1. Pipeline for selecting test data from ClinVar. The Venn diagram represents the number of variants contained within AR and AD genes, with the overlap representing variants contained in genes with more than one inheritance pattern reported in RetNet.

Table 1. Benchmarking variant classifier performance split by IRD inheritance pattern. Numbers in brackets represent AUC scores. Classifiers are ordered from highest to lowest AUC score. A full list of all classifiers tested can be found in Supplemental Table 1.

Classifier Performance [AUC]			
All AD Variants	**All AR Variants**	**Exclusive AD Haploinsufficient Variants**	**Exclusive AD Gain-of-Function and Dominant Negative Variants**
MutScore [0.969]	ClinPred [0.984]	BayesDel_addAF [0.972]	BayesDel_addAF [0.997]
MetaRNN [0.968]	MetaRNN [0.983]	MutScore [0.971]	MetaRNN [0.993]
ClinPred [0.968]	BayesDel_addAF [0.976]	ClinPred [0.968]	ClinPred [0.991]
BayesDel_addAF [0.962]	MutScore [0.963]	MetaRNN [0.964]	MutScore [0.972]
REVEL [0.943]	REVEL [0.954]	REVEL [0.961]	REVEL [0.964]
VEST4 [0.928]	VEST4 [0.934]	VEST4 [0.941]	VEST4 [0.943]
SIFT [0.892]	Polyphen2 [0.876]	Polyphen2 [0.909]	SIFT [0.875]
Polyphen2 [0.879]	CADD [0.874]	SIFT [0.905]	CADD [0.844]
CADD [0.846]	SIFT [0.863]	CADD [0.878]	Polyphen2 [0.796]

BayesDel_addAF, MetaRNN, ClinPred, and VEST4, classified the c.166G>A variant in *NR2E3* as LP, while REVEL classified it as VUS. MEP_275 has non-consanguineous English, Welsh, and Irish (White/Caucasian) ancestry and reports a family history suggestive of dominant disease. Clinically, MEP_275 presents with severe constriction of visual fields in both eyes. Fundoscopy and optical coherence tomography (OCT) reveals severe outer retinal attenuation with foveal sparing (Fig. 4B). The identified variant in *NR2E3* (c.166G>A; p.Gly56Arg) has been reported previously to cause AD RP, early onset night blindness with visual field loss, and early onset cataracts [17, 18]. Therefore, this variant in *NR2E3* serves as a positive control to demonstrate that using a combination of new variant classifier tools can correctly identify cases of AD IRDs.

Our method of utilizing a majority vote from top-performing variant classifiers also led us to identify uncharacterized missense variants linked to AD IRDs. MEP_007 and RSA_RP_018 both harbored the same heterozygous variant in exon 5 of *GUCA1A* (HGNC:4678, NM_000409: c.428T>C), with both families appearing to be affected by a dominant condition consistent

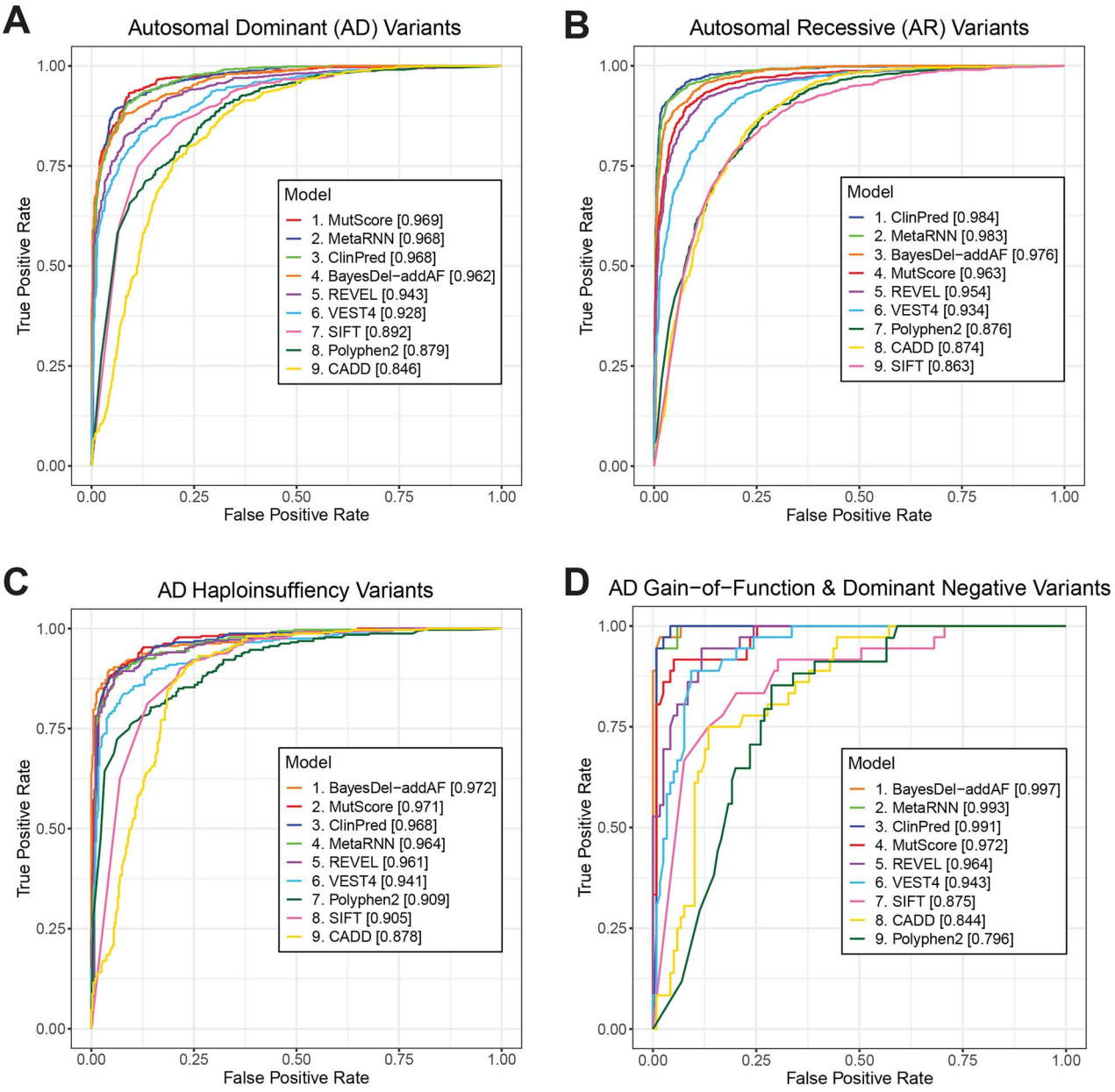

Figure 2. Performance of the top six best-performing classifiers per inheritance pattern. Performance was assessed using annotated ClinVar variants and top-performing classifiers were compared to the traditionally used tools, Polyphen2, SIFT, and CADD. (A) Classifier performance on all 1524 variants within AD genes and (B) all 2392 variants within AR genes, including variants in genes with multiple reported inheritance patterns. (C) Classifier performance using 728 variants exclusively within AD haploinsufficiency genes and (D) 156 variants within either AD gain-of-function or dominant negative genes.

with *GUCA1A*-related retinopathy (Fig. 4C and E). MEP_007 is a 53-year-old female diagnosed with cone-rod dystrophy (OMIM: 602093) with a paternal family history of blindness secondary to high myopia. Myopia has been reported for patients affected by *GUCY2D* (HGNC:4689) variants and *GUCA1A* variants have been previously associated with hyperopia [19]. Given the paternal family history of blindness secondary to high myopia spanning four generations and the proband's cone-rod dystrophy, it is suggestive that the proband is affected by an AD IRD. The heterozygous c.428T>C missense variant in exon 5 of *GUCA1A*, shown in the IGV plot (Supplemental Fig. 3B), replaces a highly conserved isoleucine residue with threonine at codon 143 (NP_000400: p.Ile143Thr). This variant has an allele frequency of $4.6e^{-6}$ using the gnomAD database, which was deemed rare. Three out of six top-performing classifiers (MetaRNN, ClinPred, and VEST4) classified the c.428T>C variant in *GUCA1A* as LP, while the remaining three (MutScore, BayesDel_addAF, and REVEL), classified it as a VUS. MEP_007 has German, Scottish, and Irish ancestry that was negative for consanguinity. Like the proband's family members, MEP_007 also has high myopia. The proband's 29-year-old son is similarly affected with high myopia which is progressive in nature. Fundoscopic images and OCT scans reveal loss of outer retinal elements in the fovea and, to a lesser degree, the perifoveal region. (Fig. 4D). A second participant, RSA_RP_018 harbored the same c.428T>C; p.Ile143Thr variant in *GUCA1A* (Supplemental Fig. 3C). RSA_RP_018 has white or Caucasian ancestry and reports progressive light sensitivity loss for 18 years and difficulty adjusting from bright to dim

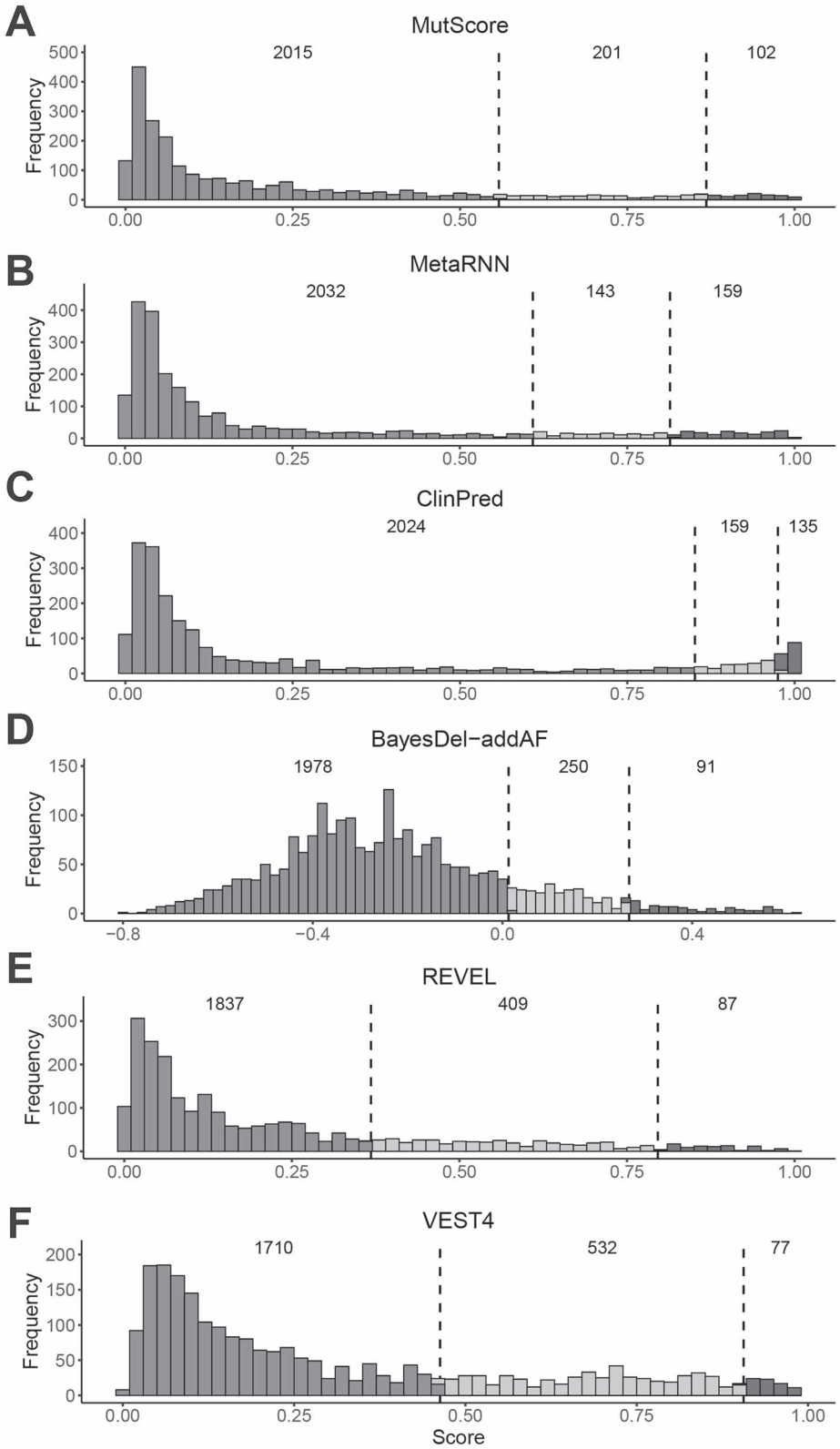

Figure 3. Pathogenicity distribution of IRD participant variants for the top six best-performing classifiers. The pathogenicity distrubutions include (A) MutScore, (B) MetaRNN, (C) ClinPred, (D) BayesDel-addAF, (E) REVEL, and (F) VEST4. Pathogenicity scores are plotted on the x-axis, with higher scores representing increasing likelihood that a variant is pathogenic. Left dashed lines represent the threshold for likely-benign (LB) variants and right dashed lines represent the threshold for likely-pathogenic (LP) variants, with variants between the two dashed lines representing variants of unknown significance (VUS).

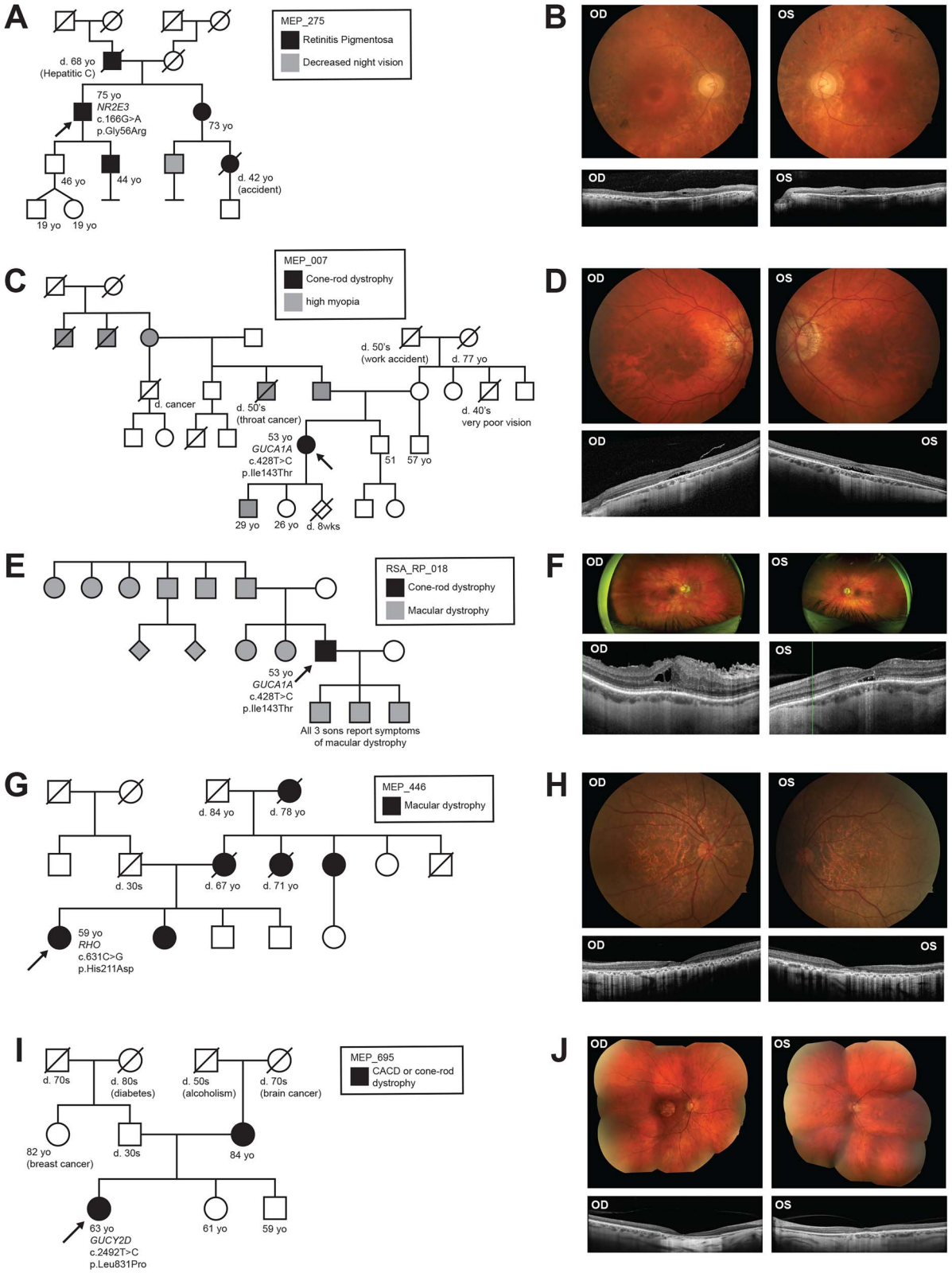

Figure 4. Pedigrees and retinal imaging for probands likely affected with AD IRDs. (A) Pedigree of MEP_275 showcasing family members affected by retinitis pigmentosa (black) and decreased night vision (grey). The proband harbors a heterozygous c.166G>A, p.Gly56Arg variant in *NR2E3*. (B) Fundoscopic and OCT images for the MEP_275's right (OD) and left (OS) retinas. (C) Pedigree of MEP_007 displaying the proband affected by cone-rod dystrophy (black) and family members affected by blinding high myopia (grey). The proband exhibits a heterozygous c.428T>A, p.Ile143Thr variant in *GUCA1A*. (D) Fundoscopic and OCT images for MEP_007. (E) Pedigree of RSA_RP_018 affected by cone-rod dystrophy (black) who harbored the same c.428T>A, p.Ile143Thr variant in *GUCA1A*. Family members affected by macular dystrophy are shown in grey, including the probands' three sons who experience symptoms of macular dystrophy. The ages and vital status of other family members in this proband's pedigree were not known. (F) Optos color fundus photography images and OCT images for RSA_RP_018. (G) Pedigree of MEP_446 displaying family members affected by retinitis pigmentosa (black). The proband shows a heterozygous c.631C>G, p.His211Asp variant in *RHO*. (H) Fundoscopic and OCT images of MEP_446's retinas. (I) Pedigree of MEP_695 showcasing the proband and their mother who have the differential diagnosis of CACD or cone-rod dystrophy. The proband has a heterozygous c.2492T>C, p.Leu831Pro variant in *GUCY2D*. (J) Montage fundoscopic images and OCT images of MEP_695's right and left retinas.

Table 2. IRD probands with pedigrees suggestive of AD inheritance patterns. Superscripts in the "protein variant" column denote previous references that report variant(s) affecting the same amino acid position within the protein. "Classifier LP Rankings" represent the number of variant classifiers that labelled the variant as likely-pathogenic (LP), out of the six top-performing tools. The "score IQR" column represents the interquartile range of output scores from the top-six performing tools. A complete list of candidate participants is reported in Supplemental Fig. 2.

Proband ID	Proband Diagnosis	Gene	cDNA Variant	Protein Variant	Protein Domain	Conservation	gnomAD Allele Frequency	Classifier LP Rankings	Score IQR
MEP_007	Cone-rod dystrophy	GUCA1A	NM_000409.5 c.428T>C	p.Ile143Thr[a]	EF-hand 4 domain	101/102	4.06256E-06	3 out of 6	0.8–0.904
RSA_RP_018	Cone-rod dystrophy	GUCA1A	NM_000409.5 c.428T>C	p.Ile143Thr[a]	EF-hand 4 domain	101/102	4.06256E-06	3 out of 6	0.8–0.904
MEP_695	Central Areolar Choroidal Dystrophy vs. Cone Dystrophy OD > OS	GUCY2D	NM_000180.4c.2492T>C	p.Leu831Pro[b]	Conserved alpha helix which forms part of the putative dimerization domain.	102/102	0	6 out of 6	0.88–0.988
MEP_275	Retinitis Pigmentosa	NR2E3	NM_014249.4c.166G>A	p.Gly56Arg[c]	C4 zinc finger in DNA-binding domain, containing P-box for half-site sequence recognition	92/98	0	5 out of 6	0.852–0.976
MEP_446	Macular Dystrophy and Familial Dominant Drusen	RHO	NM_000539.3c.631C>G	p.His211Asp[d]	Transmembrane helix H5	101/102	0	5 out of 6	0.851–0.941

References: [a]Zanolli *et al*, 2020 (PMID: 32141364). [b]Birtel *et al*, 2018 (PMID: 29555955), Gliem *et al*, 2020 (PMID: 32646556). [c]Coppieters *et al*, 2007 (PMID: 17564971). [d]Uncharacterized with same position reported previously, Keen *et al*, 1991 (PMID: 1765377).

conditions. RSA_RP_018 was also diagnosed with cone-rod dystrophy. RSA_RP_018's two sisters and paternal side of the family are significant for macular dystrophy. Additionally, the proband's three sons all report symptoms of macular dystrophy. Ultrawide field pseudocolor fundus photos showed both eyes with peripapillary atrophy, waxy pallor, and thinning of retinal vasculature (Fig. 4F). Fluorescein angiography of both eyes at arteriovenous phase showed macular hyperfluorescence corresponding to cystoid macular edema detected on OCT. The identified variant (c.428T>C; p.Ile143Thr) in *GUCA1A* has been reported once as an LP variant linked to cone dystrophy by Zanolli *et al* [20]; however, this is the first time that detailed phenotypes and inheritance patterns have been reported for people harboring this variant.

Proband MEP_446 displayed a pedigree suggestive of AD disease and harbored a heterozygous variant in exon 3 of *RHO* (HGNC:10012, NM_000539: c.631C>G) (Fig. 4G). MEP_446 is a 59-year-old female diagnosed with macular dystrophy with maternal family history significant for macular dystrophy (likely OMIM: 610445 or OMIM: 613731). Five females in the proband's family were diagnosed with early onset macular dystrophy, including one sister, the proband's mother, two aunts, and the proband's maternal grandmother. The c.631C>G variant replaces a highly conserved histidine residue with aspartic acid at codon 211 (NP_000530: p.His211Asp) in the transmembrane helix H5 of *RHO* (Supplemental Fig. 3D). The allele frequency associated with this position was zero as assessed in gnomAD. The c.631C>G variant was predicted to be LP by five out of six top-performing classifiers (MutScore, BayesDel_addAF, MetaRNN, ClinPred, and VEST4), while REVEL predicted a VUS. MEP_446 has Yupik Eskimo ancestry that was negative for consanguinity. Family history includes dominant drusen, with affected family members experiencing macular degeneration starting their 40's. Fundoscopic and OCT imaging reveals posterior pole atrophy that involves the peripapillary retina oculi uterque (OU) (Fig. 4H). Interestingly, AD retinitis pigmentosa has previously exhibited an association with c.632A>G variants in *RHO*, inducing a codon alteration at the same 211 position, except replacing the histidine residue with arginine (p.His211Arg) [21, 22]. This marks the first instance which associates macular dystrophy to the c.631C>G, p.His211Asp variant in *RHO*.

Proband MEP_695 displayed a potential AD IRD and harbored a heterozygous variant in exon 13 of *GUCY2D* (HGNC:4689, NM_000180: c.2482T>C) (Fig. 4I). MEP_695 is a 63-year-old female with non-consanguineous Norwegian, Scandinavian, and Swedish ancestry that displayed the differential diagnosis of central areolar choroidal dystrophy (CACD, OMIM: 215500) or cone-rod dystrophy (OMIM: 601777). Exam findings were consistent with CACD; however, cone dysfunction was present on full field electroretinogram, suggesting a cone dystrophy. The proband's mother is likely affected by the same condition, suggesting a potential AD inheritance pattern. CACD is often associated with *PRPH2* (HGNC:9942) variants, specifically Arg142Trp, Arg172Trp, and Arg172Gln [23–25]. MEP_695 did not have any *PRPH2* variants. On the other hand, there are several reports of AD cone-rod dystrophy linked to variants in *GUCY2D* [26, 27]. Most *GUCY2D*

variants linked with AD cone-rod dystrophy involve variants which alter codon 838, changing a highly conserved arginine residue to either proline or serine. MEP_695 had a heterozygous c.2482T>C variant which replaces a highly conserved leucine residue at codon 831 with proline (NP_000171: p.Leu831Pro) (Supplemental Fig. 3E). The allele frequency associated with the c.2482T>C variant was zero as assessed in gnomAD and was predicted as LP by six out of six top-performing classifiers (MutScore, BayesDel_addAF, MetaRNN, ClinPred, REVEL, and VEST4). The heterozygous c.2482T>C, p.Leu831Pro variant in *GUCY2D* has been previously associated with cases of cone-rod dystrophy [28, 29], albeit without comprehensive elaboration. Montage fundoscopic imaging and OCT imaging reveal large areas of macular atrophy and outer retinal attenuation of the macula, with the OD retina affected more than OS (Fig. 4J).

Discussion

In this study, we aimed to address the challenges in accurately classifying disease-causing variants associated with AD IRDs. AD diseases have a highly heterogenous range of molecular characteristics and phenotypic expression patterns across several generations, underscoring the need for accurate genetic diagnostics to guide patient treatment and family planning. Several variant classifiers exist to predict the likelihood of pathogenicity; however, it is unclear which tools should be selected for optimal classification of AD IRD-associated variants. We benchmarked 39 variant classifiers on a curated dataset of over 3000 labelled variants from ClinVar associated with IRDs, split according to inheritance pattern from RetNet [1]. Our analysis identified MutScore [11], MetaRNN [13], ClinPred [14], BayesDel_addAF [12], REVEL [15], and VEST4 [30] as the top-performing classifiers. Through rigorous threshold refining, we established criteria for categorizing variants as LP, VUS, or LB for each classifier. Previously, we leveraged WGS to identify unreported pathogenic variants in participants with IRDs [2]. Applying the top-performing classifier models and threshold criteria to the same cohort of over 1000 participants with unsolved IRDs revealed a subset of participants with AD inheritance patterns. Our findings highlight the effectiveness of reassessing variant classifiers as technologies improve and using a multi-classifier approach to accurately identify uncharacterized pathogenic variants associated with rare AD IRDs.

In agreement with our hypothesis, newer missense classifiers outperformed tools traditionally used in clinical practice, such as PolyPhen-2 [8], SIFT [9], and CADD [10]. Our results align with previous studies that benchmarked variant classifier tools by employing different filters of the ClinVar database [16, 31–34]. Newer tools and metapredictors outperformed traditionally used tools in every inheritance pattern tested (Fig. 2). When benchmarking variants in AD genes in aggregate, MutScore displayed the highest accuracy with an AUC of 0.969. This subset of IRD variants included genes linked with both AD and AR phenotypes. Genes such as *NR2E3* and *GUCY2D* are known to cause different diseases depending on whether the variant triggered a loss-of-function (LOF) or alternative protein function. For example, *NR2E3* is linked to both AD retinitis pigmentosa in people with the c.166G>A (p.Gly56Arg) variant like MEP_275, and AR enhanced S-cone syndrome in variants occurring elsewhere in the gene (Fig. 4A and B) [17]. Similarly in *GUCY2D,* the c.2513G>A (p.Arg838His) variant is associated with an AD GOF form of cone-rod dystrophy [35], while variants in other parts of the gene are known to cause AR LOF Leber congenital amaurosis [36]. When filtering out genes with overlapping AR and AD inheritance patterns, we noted that BayesDel_addAF had the best performance in AD haploinsufficiency and AD GOF & DN genes, with an AUC of 0.972 and 0.997, respectively. This accuracy in predicting rare variants in AD GOF & DN genes was unexpected, as the majority of labelled training data falls within LOF AR or AD-haploinsuffiency genes [6]. Newer tools and metapredictors had the largest improvement from traditionally used tools when classifying AD GOF & DN variants. Due to GOF and DN appearing similar with low pLI scores and low allele frequency, our method was unable to distinguish between these two mechanisms of AD disease without detailed biochemical studies. Features used in newer classifiers, such as allele frequency, residue-specific functional data such as dimerization sites, active sites, disulfide bond formation, and variant clustering within known functional domains may serve as an explanation for their improved accuracy when predicting AD GOF & DN variants [11, 31]. It is notable that BayesDel exhibited higher performance when including allele frequency (BayesDel_addAF) than when excluding it (BayesDel_noAF) (Supplemental Table 1). This can be explained by the fact that variants with high allele frequency might not be representative of rare AD variants tested in this study [37]. BayesDel is a metapredictor that uses a weighted product of likelihood ratios to estimate the overall deleteriousness of a variant, with the option to include allele frequencies gathered from ExAC and the 1000 Genomes Project. BayesDel_addAF's improved performance suggests that allele frequency is an important input variable when predicting rare AD variants.

To label variants as likely-pathogenic (LP), VUS, or likely-benign (LB), our threshold criteria for classifying variants was particularly stringent. Variant predictor tools commonly have developer-recommended pathogenicity thresholds, depending on training methods. Classifiers such as ClinPred, REVEL, and MutScore utilize random forest algorithms and report pathogenicity scores on a scale of 0–1, with 1 representing high likelihood that a variant is pathogenic. It is common to use an LP threshold of > 0.50. However, these developer-recommended thresholds were determined without distinguishing between types of inheritance pattern (AR or AD) or variant mechanism, such as LOF or GOF [38]. Using uncalibrated thresholds to determine pathogenicity/benignity classifications can result in large numbers of false positives [39]. Previous reports describe improved variant classification when pathogenicity thresholds were recalibrated using disease-specific cohorts [34, 40] or gene-specific attributes [41]. Since a gene-specific approach is not applicable to rare AD variants with little to no prior documentation, we adopted a disease-specific approach (IRDs) split by inheritance pattern. We developed stringent thresholds, representing the point at which 95% of variants were accurately classified as either PLP or BLB (Fig. 3). Instead of using a consensus approach, where all tools had to result in the same prediction, we used a majority vote system. The guidelines created by the American College of Medical Genetics recommend using a multi-classifier consensus approach [42]; however, this may cause lower sensitivity than using a majority-voting system [31]. There exists a balancing act between improved sensitivity/specificity and the likelihood of missing a few true positives. The trade-off also impacts the generation of false positives and VUS, influencing the overall clinical utility of using tools with less strict thresholds. It is important to minimize VUS as ambiguous genetic testing can lead to psychological distress in patients [43].

We observed that metapredictors, such as BayesDel, MetaRNN, ClinPred, and MutScore, achieved comparable high performance, supporting previously observed findings that metapredictors contain significant overlap and have improved performance when

compared to their individual components [31, 32, 44]. Therefore, some authors recommend adjusting the American College of Medical Genetics guidelines from using a multi-classifier consensus approach to utilizing just one metapredictor [31, 34]. Metapredictor tools often utilize the same input variables, such as scores from older classifiers like CADD and Polyphen-2, supporting the claim for a singular model. However, if a singular model were to be used and found to be incorrect, it may set back the correct diagnosis in some patients. Furthermore, different tools utilize different machine learning methods, such as MutScore using a random forest model and MetaRNN using a recurrent neural network. Various computational approaches may be better suited for certain diseases and inheritance patterns. Our majority-vote approach strikes a middle ground by minimizing VUS while increasing the confidence of true positive pathogenic variants by including multiple scores from tools which utilized different computational methods. If a single model were to be used, we recommend threshold refining via Bayesian reasoning to generate posterior probabilities for calculating odds of pathogenicity as reported previously [45]. Pejaver *et al* [39] utilized posterior probabilities to calibrate several missense classifiers, defining threshold intervals for four levels of confidence for both benign and pathogenic labels. These threshold intervals included: very strong, strong, moderate, and supporting for likelihood of pathogenicity/benignity. While no tools reached threshold criteria supporting "very strong" evidence for pathogenicity, we found that our 95% accuracy thresholds ranged between the "moderate" and "strong" levels for support. Using a single high-performing metapredictor with multiple levels of confidence thresholds supporting pathogenicity/benignity is a promising alternative to our approach which used multiple classifiers calibrated to strict LP/VUS/LB classifications.

Despite the rarity of labelled AD variants, newer tools yielded high performance and successfully identified previously documented variants along with uncharacterized variants in our IRD cohort. Analysis of our cohort of undiagnosed IRD participants yielded 22 candidate participants harboring LP variants in AD genes, representing 2.2% of total participants. Our approach demonstrated accurate classification of known AD pathogenic variants in *NR2E3* and *GUCY2D*, and uncharacterized variants in *GUCA1A* and *RHO*. The c.166G>A (p.Gly56Arg) variant in *NR2E3* and the c.2482T>C (p.Leu831Pro) variant in *GUCY2D* serves as confirmation that our approach accurately identified known variants associated with AD disease (Fig. 4A and B, I and J) [17, 18, 28, 29]. The uncharacterized variants in *GUCA1A* and *RHO* were found either in proximity to established pathogenic variants or within protein domains indicative of AD disease. We describe two participants with the same c.428T>C (p.Ile143Thr) variant in *GUCA1A* (Fig. 4C–F). Notably, there exists a 3-base-pair insertion one base pair upstream of the c.428T>C variant; however, it was predicted to be benign using the MetaRNN tool for insertions-deletions (InDels). Three out of six tools labeled the c.428T>C variant in *GUCA1A* as LP, while the other three tools labelled it VUS. The c.428T>C variant changes a highly conserved isoleucine residue to threonine at position 143 within the protein's EF-hand 4 domain, which is adjacent to other variants linked to AD cone-rod dystrophy at positions 144, 148, 151, and 159 [46–48]. The c.631C>G (p.His211Asp) variant in *RHO* replaces a highly conserved histidine residue with aspartic acid at position 211 within the protein's transmembrane helix H5 domain (Fig. 4G and H). A different amino acid change at the same 211 position (p.His211Arg) has been previously associated with AD retinitis pigmentosa [21]. Considering that the c.631C>G (p.His211Asp) variant in *RHO* occurred at the identical amino acid position, inducing a change in amino acid charge, coupled with the significant family history of maternally-inherited AD macular degeneration, we assert that this variant is likely associated with this participant's observed AD IRD. Our results are encouraging because there are currently over 40 active clinical trials for ocular diseases using AAV gene therapy [49]. One modifier gene therapy, OCU400 (Ocugen, Inc.), aims to treat people with AD *NR2E3* and AD *RHO* variants (NCT05203939) [50]. Building on the promising landscape of ongoing clinical trials, our approach employing a majority vote of new variant classifier tools holds potential to expedite the diagnosis of patients with AD IRDs, facilitating more accurate molecular prediction.

There are limitations to our method of classifying AD variants in IRD participants. Notably, several new metapredictor tools utilized the growing ClinVar database for model training. Given the substantial training data provided by ClinVar, it is unsurprising that newer metapredictors outperform older tools, such as SIFT and Polyphen-2, which were created before ClinVar. Metapredictors released more recently, such as MutScore, are expected to have improved performance compared to older metapredictors like REVEL simply due to more comprehensive training datasets. A constraint for accessing variant prediction tools is including training data while testing a tool's performance. We controlled for this constraint by filtering ClinVar variants by date of submission, filtering out all training variants from the testing phase of this study. Another limitation is that current tools perform poorly when predicting whether a variant will behave in an AD or AR manner [51]. In this study, we used the RetNet database which collects phenotypes for each reported IRD gene. We used RetNet to group variants into genes with different reported inheritance patterns, validating the predicted inheritance pattern after conducting variant classification through pedigree analysis. However, people harboring variants that arise *de-novo*, or as a result of somatic or gonadal mosaicism, will present without significant family history of disease [52]. Adopted individuals with no biological family history and genes that have variable expressivity or incomplete penetrance make validation challenging. However, even without validation via pedigree, this does not rule out the possibility of *de-novo* variants acting in an AD manner. Based on the demonstrated high accuracy of newer variant classifier tools, our approach of classifying AD variants remains valuable for genetic counseling in people without significant family histories of IRDs. It is important to provide family planning services to individuals presumed to harbor *de-novo* likely pathogenic AD variants, ensuring they are well-informed about the associated risks and potential treatments for their offspring. To avoid constraints involving limited family history data or limited training data due to the rarity of AD variants, novel prediction methods, such as EVE [53], AlphaMissense [54], and ESM1b [55] may offer innovative solutions to predicting new variants. The evolutionary model of variant effect (EVE) uses deep generative models to predict variant pathogenicity by modeling the distribution of sequence variation across organisms, highlighting the importance of conserved protein sequences that maintain fitness. This method eliminates much of the need for extensive training datasets, which may be sparse for rare AD variants. AlphaMissense combines evolutionary data with protein structural predictions from AlphaFold to predict a variant's effect on overall protein function. ESM1b is a large protein language model which includes isoform specificity in variant prediction, improving prospects for generalizability for rare diseases. These new tools are useful for addressing the pitfalls of using machine learning-based metapredictors, namely that they are less reliant on labelled datasets, which in the case

of rare AD variants, may lead to overfitting and limited generalizability. We recommend making these tools widely available by standardizing their input variables and by integrating them in centralized variant annotation databases, such as dbNSFP used by ANNOVAR, to make comparisons between tools more seamless.

In conclusion, our study provides a foundation for improved precision in the genetic diagnosis of AD IRDs, a crucial step for advancing targeted therapeutic interventions and guiding patient care. Leveraging a multi-classifier approach consisting of newer metapredictors, our analysis accurately classified previously described and uncharacterized variants linked to AD IRDs in our participant cohort. Future research should calibrate pathogenicity thresholds in a disease-specific manner and utilize tools with novel prediction methods, such as EVE, AlphaMissense, and ESM1b, to yield further insight into the best-performing variant classifiers for diagnosing IRD participants. We encourage clinicians to access the efficacy of our variant classification approach in patients with suspected AD IRDs in accordance with the guidelines established by the American College of Medical Genetics.

Materials and methods

Variant selection from ClinVar by inheritance pattern

We extracted all missense short nucleotide variants (SNVs) submitted to ClinVar as of June 26th, 2023 (Fig. 1). To avoid overlap with training data, we filtered out variants submitted before November 21st, 2020, the most recent date used for training in the MutScore classifier [11]. The American College of Medical Genetics classifies variants into five categories: pathogenic, likely pathogenic, variant of unknown significance (VUS), likely benign, and benign [42]. For benchmarking classifiers, we selected variants annotated as pathogenic or likely pathogenic (PLP) or benign or likely benign (BLB). A list of documented IRD genes was obtained from RetNet [1] (https://web.sph.uth.edu/RetNet/). Functional annotation of genomic variants of known IRD genes with PLP or BLB categories was conducted using ANNOVAR (version 2023 Mar 15) [56, 57]. ANNOVAR was run using the genome build hg19 with gene-based annotation by refgene and filter-based annotations with the dbscsnv11, dbnsfp42a, and mutscore databases. From the ANNOVAR output, nonsynonymous SNVs for IRD genes were labeled with inheritance patterns from RetNet disease descriptions and literature review (Supplemental Table 3). Genes with AD inheritance patterns were considered haploinsufficient if their allele frequency was $< 1e^{-3}$ and pLI > 0.90, as described previously [58]. Variants within genes with AD inheritance patterns were considered gain-of-function (GOF) or dominant negative (DN) if their allele frequency was $< 1e^{-5}$ and pLI score < 0.90, although a range of mechanisms exist to explain why these genes function an AD manner. Several IRDs genes were associated with both AR and AD inheritance patterns. Genes linked to diseases displaying multiple inheritance patterns were categorized as following a "complex" inheritance pattern. This complexity may arise from variants occurring in distinct protein domains, contributing to diverse phenotypes and inheritance patterns.

Benchmarking classifiers and defining thresholds for pathogenicity

Benchmarking of 39 variant classifiers, with variants split by inheritance pattern, was accomplished using receiver operating characteristic (ROC) curve analysis and area under the curve scores (AUC) using the "roc_curve" and "auc" functions from the Python package scikit-learn [59]. The input consisting of variant pathogenicity scores was evaluated against the ground truth PLP/BLB labels from ClinVar. We then selected the top six best-performing classifiers for AD IRD variants. To compare the top-performing classifiers with conventional tools commonly used in clinical practice, like SIFT, CADD, and Polyphen-2, a student's t-test was conducted between classifier groups. The interquartile range (IQR) was calculated for the top-six performing classifier tools, representing pathogenicity scores from 0–1, with higher numbers denoting increased pathogenicity scores. BayesDel_addAF scores were normalized to fit the 0–1 scale to calculate IQR.

To ensure accurate categorization of participant variants, there was need to define thresholds for each classifier for which scores accurately represent pathogenicity. For each top-performing classifier, an upper and lower threshold was calculated to assess if variants were likely pathogenic (LP), variants of unknown significance (VUS), or likely benign (LB) as previously described [11]. Briefly, for a variant to be classified as LP, it had to surpass the upper score threshold representing the point at which 95% of the testing data from ClinVar was accurately confirmed as PLP. Likewise, variants were considered LB if their classifier score fell below the lower threshold where 95% of the testing data from ClinVar were classified as BLB. Variants with scores between the upper and lower thresholds were considered VUS. The code used to parse ClinVar, run ANNOVAR, and generate figures can be found on the publicly available GitHub repository: https://github.com/toofastdan117/AD_IRDs.

Variant classification of undiagnosed IRD participants

All probands in this study received clinical diagnoses of IRDs following examinations conducted by a qualified ophthalmologist. Ethics approval was done at each institution via the Baylor College of Medicine institutional review board. This study adhered to the principles outlined in the Declaration of Helsinki and obtained approval from the institutional review boards at all collaborating institutions. DNA was derived from blood samples following written informed consent by all probands. Probands' DNA samples were extracted using Qiagen blood genomic DNA extraction kits (Qiagen, Hilden, Germany). All deidentified clinical data, including fundoscopic images, optical coherence tomography, and pedigrees, were obtained by a certified ophthalmologist for participants of interest.

To identify variants in participants with IRDs, all participants underwent gene panel testing. For probands with unresolved molecular diagnoses, we performed WGS on proband DNA as reported previously [2, 60]. Briefly, WGS was conducted using an Illumina NovaSeq6000 platform with paired-end 2×150bp reads, achieving a sequencing depth of approximately 30x coverage. Data generated from WGS were processed at the Human Genome Sequencing Center at Baylor College of Medicine, utilizing a pipeline described previously [61]. NGS reads were aligned to the human genome assembly (hg19) through Burrows-Wheeler Alignment (BWA) [62]. Identification of single nucleotide variants (SNVs) and small insertion–deletion variants (InDels) was performed using GATK4 [63]. Variants that were unlikely to contribute to rare diseases were filtered out if their population frequency exceeded 0.5% in databases such as 1000Genomes [64], ExAC [65], HGVD [66], CHARGE [67], or GnomAD r2.0.1 [65]. Potential mapping and sequencing errors were addressed through manual examination of raw bam files containing candidate

variants using the Integrative Genomics Viewer (IGV) [68]. Genetic conservation was assessed using the phastCons.hg19.100way data from the UCSC Genome Browser [69].

Candidate participants were selected if a majority vote from the top-six-performing classifiers predicted an LP variant in an AD IRD gene. We visualized the majority vote process by using the pheatmap package in R to generate a heatmap clustered into three groups: LP, LB, and VUS. Variants in the LP cluster, where the classifier concordance was high, were selected for further analysis. In participants with LP variants in IRD genes, the participant's phenotype was cross checked with previous literature. If the participant's phenotype was similar to previous reports, the participant's ophthalmologists were contacted to gather pedigrees, fundoscopic images, and OCT images. Segregation testing was performed on participants with pedigrees suggesting an AD inheritance pattern. Variants in selected participants were validated with the VariantValidator tool using the GRCh17 genome build (Supplemental Table 4) [70]. We have submitted genome sequencing data for probands described in this study to the database of Genotypes and Phenotypes (dbGaP) under the study accession number phs001517.

Acknowledgements

We acknowledge Syed Haqqani and the Office of Data Science and Health Informatics at the National Eye Institute for providing additional information about patients seen at the National Institutes of Health. We would like to thank eyeGENE for providing patient samples collected at the National Eye Institute.

Author contributions

D.C.B., M.W., R.C. conceptualized and planned the experiments. D.C.B. wrote the manuscript while M.W., H.M.J.H., and R.C reviewed and edited. D.C.B., M.W., H.M.J.H., D.R., and Y.L. carried out the formal analysis by curating variants from ClinVar, gathering gene inheritance patterns from RetNet, and designing the experimental pipeline. M.M., M.E.P., P.Y., L.E., R.S.A., J.S., F.B.O.P., A.M., M.G., R.K.K., I.L., R.S., and G.Z. curated data from IRD patients by performing eye exams, imaging retinas, and collecting pedigrees. All authors provided critical feedback for the manuscript.

Supplementary data

Supplementary data is available at *HMG Journal* online.

Conflict of interest statement: All authors declare no conflicts of interest.

Funding

This work was supported by grants from the National Eye Institute [EY022356, EY018571, EY002520, P30EY010572, EY09076, EY030499]; Retinal Research Foundation; NIH shared instrument grant [S10OD023469]; the Malcolm M. Marquis, MD Endowed Fund for Innovation; the Daljit S. and Elaine Sarkaria Charitable Foundation; Unrestricted Grant from Research to Prevent Blindness; Fighting Blindness Canada; and funding from the Vision Health Research Network.

Ethics declaration

This study obtained approval from the central Institutional Review Board (IRB) at Baylor College of Medicine. All authors confirm that human research participants provided informed consent for research and publication of the data presented in this study. To ensure participant confidentiality, all individual-level and clinical data was de-identified for this study.

References

1. Daiger SP, Rossiter BJF, Greenberg J. *et al.* Data services and software for identifying genes and mutations causing retinal degeneration. *Invest Ophthalmol Vis Sci* 1998;**39**:S295. https://sph.uth.edu/RetNet/.
2. Hussain HMJ, Wang M, Huang A. *et al.* Novel pathogenic mutations identified from whole-genome sequencing in unsolved cases of patients affected with inherited retinal diseases. *Genes* 2023;**14**:447.
3. O'Sullivan J, Mullaney BG, Bhaskar SS. *et al.* A paradigm shift in the delivery of services for diagnosis of inherited retinal disease. *J Med Genet* 2012;**49**:322–6.
4. Ellingford JM, Barton S, Bhaskar S. *et al.* Whole genome sequencing increases molecular diagnostic yield compared with current diagnostic testing for inherited retinal disease. *Ophthalmology* 2016;**123**:1143–50.
5. Boycott KM, Vanstone MR, Bulman DE. *et al.* Rare-disease genetics in the era of next-generation sequencing: discovery to translation. *Nat Rev Genet* 2013;**14**:681–91.
6. Turner TN, Douville C, Kim D. *et al.* Proteins linked to autosomal dominant and autosomal recessive disorders harbor characteristic rare missense mutation distribution patterns. *Hum Mol Genet* 2015;**24**:5995–6002.
7. Garafalo AV, Cideciyan AV, Héon E. *et al.* Progress in treating inherited retinal diseases: early subretinal gene therapy clinical trials and candidates for future initiatives. *Prog Retin Eye Res* 2020;**77**:100827.
8. Adzhubei I, Jordan DM, Sunyaev SR. Predicting functional effect of human missense mutations using PolyPhen-2. *Curr Protoc Hum Genet* 2013;**76**:Unit7.20.
9. Ng PC, Henikoff S. SIFT: predicting amino acid changes that affect protein function. *Nucleic Acids Res* 2003;**31**:3812–4.
10. Kircher M, Witten DM, Jain P. *et al.* A general framework for estimating the relative pathogenicity of human genetic variants. *Nat Genet* 2014;**46**:310–5.
11. Quinodoz M, Peter VG, Cisarova K. *et al.* Analysis of missense variants in the human genome reveals widespread gene-specific clustering and improves prediction of pathogenicity. *Am J Hum Genet* 2022;**109**:457–70.
12. Feng B-J. PERCH: a unified framework for disease gene prioritization. *Hum Mutat* 2017;**38**:243–51.
13. Li C, Zhi D, Wang K. *et al.* MetaRNN: differentiating rare pathogenic and rare benign missense SNVs and InDels using deep learning. *Genome Med* 2022;**14**:115.
14. Alirezaie N, Kernohan KD, Hartley T. *et al.* ClinPred: prediction tool to identify disease-relevant nonsynonymous single-nucleotide variants. *Am J Hum Genet* 2018;**103**:474–83.
15. Ioannidis NM, Rothstein JH, Pejaver V. *et al.* REVEL: an ensemble method for predicting the pathogenicity of rare missense variants. *Am J Hum Genet* 2016;**99**:877–85.
16. Livesey BJ, Marsh JA. Updated benchmarking of variant effect predictors using deep mutational scanning. *Mol Syst Biol* 2023;**19**:e11474.
17. Coppieters F, Leroy BP, Beysen D. *et al.* Recurrent mutation in the first zinc finger of the orphan nuclear receptor NR2E3 causes autosomal dominant retinitis Pigmentosa. *Am J Hum Genet* 2007;**81**:147–57.

18. Blanco-Kelly F, García Hoyos M, Lopez Martinez MA. *et al.* Dominant retinitis Pigmentosa, p.Gly56Arg mutation in NR2E3: phenotype in a large cohort of 24 cases. *PLoS One* 2016;**11**: e0149473.
19. Zobor D, Zrenner E, Wissinger B. *et al.* GUCY2D- or GUCA1A-related autosomal dominant cone-rod dystrophy: is there a phenotypic difference? *Retina* 2014;**34**:1576–87.
20. Zanolli M, Oporto JI, Verdaguer JI. *et al.* Genetic testing for inherited ocular conditions in a developing country. *Ophthalmic Genet* 2020;**41**:36–40.
21. Macke JP, Davenport CM, Jacobson SG. *et al.* Identification of novel rhodopsin mutations responsible for retinitis pigmentosa: implications for the structure and function of rhodopsin. *Am J Hum Genet* 1993;**53**:80–9.
22. Keen TJ, Inglehearn CF, Lester DH. *et al.* Autosomal dominant retinitis pigmentosa: four new mutations in rhodopsin, one of them in the retinal attachment site. *Genomics* 1991;**11**: 199–205.
23. Renner AB, Fiebig BS, Weber BHF. *et al.* Phenotypic variability and long-term follow-up of patients with known and novel PRPH2/RDS gene mutations. *Am J Ophthalmol* 2009;**147**: 518–530.e1.
24. Wells J, Wroblewski J, Keen J. *et al.* Mutations in the human retinal degeneration slow (RDS) gene can cause either retinitis pigmentosa or macular dystrophy. *Nat Genet* 1993;**3**:213–8.
25. Neveling K, Collin RWJ, Gilissen C. *et al.* Next-generation genetic testing for retinitis pigmentosa. *Hum Mutat* 2012;**33**:963–72.
26. Gregory-Evans K, Kelsell RE, Gregory-Evans CY. *et al.* Autosomal dominant cone–rod retinal dystrophy (CORD6) from heterozygous mutation of GUCY2D, which encodes retinal guanylate cyclase11The authors have no proprietary interests in the materials mentioned in the study. *Ophthalmology* 2000;**107**: 55–61.
27. Payne AM, Morris AG, Downes SM. *et al.* Clustering and frequency of mutations in the retinal guanylate cyclase (GUCY2D) gene in patients with dominant cone-rod dystrophies. *J Med Genet* 2001;**38**:611–4.
28. Gliem M, Müller PL, Birtel J. *et al.* Quantitative fundus autofluorescence and genetic associations in macular, cone, and cone–rod dystrophies. *Ophthalmol Retina* 2020;**4**:737–49.
29. Birtel J, Eisenberger T, Gliem M. *et al.* Clinical and genetic characteristics of 251 consecutive patients with macular and cone/cone-rod dystrophy. *Sci Rep* 2018;**8**:4824.
30. Carter H, Douville C, Stenson PD. *et al.* Identifying Mendelian disease genes with the variant effect scoring tool. *BMC Genomics* 2013;**14**:S3.
31. Gunning AC, Fryer V, Fasham J. *et al.* Assessing performance of pathogenicity predictors using clinically relevant variant datasets. *J Med Genet* 2021;**58**:547–55.
32. Barbosa P, Ribeiro M, Carmo-Fonseca M. *et al.* Clinical significance of genetic variation in hypertrophic cardiomyopathy: comparison of computational tools to prioritize missense variants. *Front Cardiovasc Med* 2022;**9**:975478.
33. Cubuk C, Garrett A, Choi S. *et al.* Clinical likelihood ratios and balanced accuracy for 44 in silico tools against multiple large-scale functional assays of cancer susceptibility genes. *Genet Med* 2021;**23**:2096–104.
34. Kumaran M, Devarajan B. eyeVarP: a computational framework for the identification of pathogenic variants specific to eye disease. *Genet Med* 2023;**25**:100862.
35. Mukherjee R, Robson AG, Holder GE. *et al.* A detailed phenotypic description of autosomal dominant cone dystrophy due to a de novo mutation in the GUCY2D gene. *Eye* 2014;**28**:481–7.
36. Stunkel ML, Brodie SE, Cideciyan AV. *et al.* Expanded retinal disease Spectrum associated with autosomal recessive mutations in GUCY2D. *Am J Ophthalmol* 2018;**190**:58–68.
37. Wu Y, Li R, Sun S. *et al.* Improved pathogenicity prediction for rare human missense variants. *Am J Hum Genet* 2021;**108**: 1891–906.
38. Ramakrishnan G, Baakman C, Heijl S. *et al.* Understanding structure-guided variant effect predictions using 3D convolutional neural networks. *Front Mol Biosci* 2023;**10**:1204157.
39. Pejaver V, Byrne AB, Feng B-J. *et al.* Calibration of computational tools for missense variant pathogenicity classification and ClinGen recommendations for PP3/BP4 criteria. *Am J Hum Genet* 2022;**109**:2163–77.
40. Zhang X, Walsh R, Whiffin N. *et al.* Disease-specific variant pathogenicity prediction significantly improves variant interpretation in inherited cardiac conditions. *Genet Med* 2021;**23**: 69–79.
41. Wang M, Wei L. iFish: predicting the pathogenicity of human nonsynonymous variants using gene-specific/family-specific attributes and classifiers. *Sci Rep* 2016;**6**:31321.
42. Richards S, Aziz N, Bale S. *et al.* Standards and guidelines for the interpretation of sequence variants: a joint consensus recommendation of the American College of Medical Genetics and Genomics and the Association for Molecular Pathology. *Genet Med* 2015;**17**:405–24.
43. Mighton C, Shickh S, Uleryk E. *et al.* Clinical and psychological outcomes of receiving a variant of uncertain significance from multigene panel testing or genomic sequencing: a systematic review and meta-analysis. *Genet Med* 2021;**23**:22–33.
44. Tian Y, Pesaran T, Chamberlin A. *et al.* REVEL and BayesDel outperform other in silico meta-predictors for clinical variant classification. *Sci Rep* 2019;**9**:12752.
45. Tavtigian SV, Greenblatt MS, Harrison SM. *et al.* Modeling the ACMG/AMP variant classification guidelines as a Bayesian classification framework. *Genet Med* 2018;**20**:1054–60.
46. Kitiratschky VBD, Behnen P, Kellner U. *et al.* Mutations in the GUCA1A gene involved in hereditary cone dystrophies impair calcium-mediated regulation of guanylate cyclase. *Hum Mutat* 2009;**30**:E782–96.
47. Tang S, Xia Y, Dai Y. *et al.* Functional characterization of a novel GUCA1A missense mutation (D144G) in autosomal dominant cone dystrophy: a novel pathogenic GUCA1A variant in COD. *Mol Vis* 2019;**25**:921–xxx.
48. Manes G, Mamouni S, Hérald E. *et al.* Cone dystrophy or macular dystrophy associated with novel autosomal dominant GUCA1A mutations. *Mol Vis* 2017;**23**:198–209.
49. Tian B, Bilsbury E, Doherty S. *et al.* Ocular drug delivery: advancements and innovations. *Pharmaceutics* 2022;**14**:1931.
50. Drag S, Dotiwala F, Upadhyay AK. Gene therapy for retinal degenerative diseases: progress, challenges, and future directions. *Invest Ophthalmol Vis Sci* 2023;**64**:39.
51. Zschocke J, Byers PH, Wilkie AOM. Mendelian inheritance revisited: dominance and recessiveness in medical genetics. *Nat Rev Genet* 2023;**24**:442–63.
52. Legrand A, Devriese M, Dupuis-Girod S. *et al.* Frequency of de novo variants and parental mosaicism in vascular Ehlers-Danlos syndrome. *Genet Med* 2019;**21**:1568–75.
53. Frazer J, Notin P, Dias M. *et al.* Disease variant prediction with deep generative models of evolutionary data. *Nature* 2021;**599**: 91–5.
54. Cheng J, Novati G, Pan J. *et al.* Accurate proteome-wide missense variant effect prediction with AlphaMissense. *Science* 2023; **381**:eadg7492.

55. Brandes N, Goldman G, Wang CH. *et al.* Genome-wide prediction of disease variant effects with a deep protein language model. *Nat Genet* 2023;**55**:1512–22.
56. Wang K, Li M, Hakonarson H. ANNOVAR: functional annotation of genetic variants from high-throughput sequencing data. *Nucleic Acids Res* 2010;**38**:e164.
57. Yang H, Wang K. Genomic variant annotation and prioritization with ANNOVAR and wANNOVAR. *Nat Protoc* 2015;**10**:1556–66.
58. Lek M, Karczewski KJ, Minikel EV. *et al.* Analysis of protein-coding genetic variation in 60,706 humans. *Nature* 2016;**536**:285–91.
59. Pedregosa F, Varoquaux G, Gramfort A. *et al.* Scikit-learn: machine learning in python. *J Mach Learn Res* 2011;**12**:2825–30.
60. Wen S, Wang M, Qian X. *et al.* Systematic assessment of the contribution of structural variants to inherited retinal diseases. *Hum Mol Genet* 2023;**32**:2005–15.
61. Soens ZT, Li Y, Zhao L. *et al.* Hypomorphic mutations identified in the candidate Leber congenital amaurosis gene CLUAP1. *Genet Med* 2016;**18**:1044–51.
62. Li H, Durbin R. Fast and accurate short read alignment with burrows-wheeler transform. *Bioinformatics* 2009;**25**:1754–60.
63. McKenna A, Hanna M, Banks E. *et al.* The genome analysis toolkit: a MapReduce framework for analyzing next-generation DNA sequencing data. *Genome Res* 2010;**20**:1297–303.
64. Durbin RM, Altshuler D, Durbin RM. *et al.* A map of human genome variation from population-scale sequencing. *Nature* 2010;**467**:1061–73.
65. Karczewski KJ, Weisburd B, Thomas B. *et al.* The ExAC browser: displaying reference data information from over 60 000 exomes. *Nucleic Acids Res* 2017;**45**:D840–5.
66. Higasa K, Miyake N, Yoshimura J. *et al.* Human genetic variation database, a reference database of genetic variations in the Japanese population. *J Hum Genet* 2016;**61**:547–53.
67. Psaty BM, O'Donnell CJ, Gudnason V. *et al.* Cohorts for heart and aging research in genomic epidemiology (CHARGE) consortium: design of prospective meta-analyses of genome-wide association studies from five cohorts. *Circ Cardiovasc Genet* 2009;**2**:73–80.
68. Robinson JT, Thorvaldsdóttir H, Winckler W. *et al.* Integrative genomics viewer. *Nat Biotechnol* 2011;**29**:24–6.
69. Pollard KS, Hubisz MJ, Rosenbloom KR. *et al.* Detection of nonneutral substitution rates on mammalian phylogenies. *Genome Res* 2010;**20**:110–21.
70. Freeman PJ, Hart RK, Gretton LJ. *et al.* VariantValidator: accurate validation, mapping, and formatting of sequence variation descriptions. *Hum Mutat* 2018;**39**:61–8.